Improved calculation of $W^{\pm}H^{\mp}$ associated production via gluon-gluon fusion at the CERN LHC

Zhou Fei,[2] Ma Wen-Gan,[1,2] Jiang Yi,[2] Han Liang,[2] and Wan Lang-Hui[2]
[1]*CCAST (World Laboratory), P.O. Box 8730, Beijing 100080, China*
[2]*Department of Modern Physics, University of Science and Technology of China (USTC), Hefei, Anhui 230027, China*
(Received 11 July 2000; revised manuscript received 30 August 2000; published 21 November 2000)

The production process for the charged Higgs boson associated with the *W* boson via gluon-gluon fusion at the CERN large hadron collider (LHC) in the minimal supersymmetric standard model (MSSM) is investigated with one-loop diagrams of both quarks and scalar quarks. We find the contribution from the scalar quark loops can be comparable with those from quark loop diagrams and could decrease or enhance the cross section substantially in some parameter space. The results show that this cross section can be about 45 fb with our chosen input parameters at the CERN LHC. The analysis of the p_T distribution shows that the line shapes partly depend on the virtual scalar quark contributions. The numerical analysis of their production rates is also carried out in the minimal supergravity (MSUGRA) scenario. We find that the supersymmetric contributions can reach $+56\%$ of the total cross section in the MSUGRA-inspired MSSM.

DOI: 10.1103/PhysRevD.63.015002 PACS number(s): 12.60.Jv, 12.15.Lk, 12.60.Fr, 13.85.−t

I. INTRODUCTION

The minimal standard model (MSM) [1,2] has been confirmed by experiments as a very successful model of particle physics in the past decades. But until now the symmetry-breaking structure of the electroweak interactions has not yet been directly explored experimentally. Therefore the exploration of additional Higgs bosons will be very important in probing the extended Higgs sector. As we know, any enlargement of the Higgs sector beyond the single $SU(2)_L$ Higgs doublet of the MSM necessarily involves charged Higgs bosons. Like the general two-Higgs-doublet model, the minimal supersymmetric standard model (MSSM) [3–5] also has two Higgs doublets and includes charged Higgs bosons, which is not involved in the MSM. Therefore, experimental discovery of a charged Higgs boson $H^{\pm}$ will be the direct verification of these extended versions of the Higgs sector.

In the future multi-TeV hadron colliders such as the CERN large hadron collider (LHC), the search for the charged Higgs bosons and other neutral Higgs bosons, and the study of their nature are the most important tasks. At hadron colliders, there are several mechanisms which can produce charged Higgs bosons [6]. If $m_{H^{\pm}}<m_t-m_b$, the charged Higgs bosons can abundantly be produced in decays of top quarks (top antiquarks) $[t\bar{t}\to bH^+(\bar{b}H^-)]$ produced by a parent production channel $pp\to t\bar{t}$; i.e., the LHC experimenters will never need to resort to $pp\to W^{\pm}H^{\mp}$ associated production for charged Higgs boson searches. The dominant decay channels in this mass range are $H^+(H^-)\to\bar{\tau}\nu_{\tau}(\tau\bar{\nu}_{\tau})$. For the large mass charged Higgs bosons, the $H^{\pm}$ bosons are mainly produced by $gb(g\bar{b})\to tH^-(\bar{t}H^+)$ [7], $gg\to t\bar{b}H^-(\bar{t}bH^+)$ [8], and $qb(\bar{q}b)\to q'bH^+(\bar{q}'\bar{b}H^+)$ [9]. The sequential decays $H^+\to t\bar{b}$ are known as a preferred channel for charged Higgs boson search. But these signal processes appear together with large QCD background. The charged Higgs boson pair can be produced by the Drell-Yan process $q\bar{q}\to H^+H^-$ [10] and gluon-gluon fusion at one-loop $gg\to H^+H^-$ [11] at the LHC. Since the heavy $H^{\pm}$ bosons decay dominantly into quark pairs, the pair production process is always accompanied by serious QCD backgrounds too. Therefore, the production of the heavy charged Higgs bosons associated with $W^{\pm}$ bosons seems to be an attractive way of searching for the $H^{\pm}$ bosons, because the $W^{\pm}$ boson's leptonic decay may be used as a spectacular trigger. From above discussion, we can see that the phenomenological relevance of $pp\to(b\bar{b},gg)\to W^{\pm}H^{\mp}+X$ only really applies to the case of heavy charged Higgs states when $m_{H^{\pm}}>m_t+m_b$.

Recently Moretti and Odagiri found that the simileptonic signature ''$b\bar{b}W^+W^-\to b\bar{b}jjl+$missing momentum'' is dominated by $t\bar{t}$ events [12]. It seems that it may be hard to disentangle the $W^{\pm}H^{\mp}$ signal in the decay mode of the heavy charged Higgs boson $H^+\to t\bar{b}$ at the LHC. In Ref. [12] they stressed also that charged Higgs boson production in association with $W^{\pm}$ at hadron colliders, represents a novel mechanism, whose decay phenomenology is largely unknown and that should be investigated further. Therefore one may consider the possible dominant MSSM decay channels of the heavy charged Higgs bosons, involving squarks, sleptons, and gauginos, as signal processes.

The production of charged Higgs bosons in association with *W* gauge bosons at the LHC involves several subprocess both at the tree and one-loop level. In [13] Dicus *et al.* numerically calculated these association productions at hadron colliders for vanished bottom quark mass. These processes in the MSSM are further studied by Barrientos Bendezu and Kniehl in Refs. [14,15]. In above references the authors ignored the contributions from the squark loop diagrams for the subprocess $gg\to W^{\pm}H^{\mp}$, and their results show that the cross section contributed by the tree-level subprocess $b\bar{b}\to W^{\pm}H^{\mp}$ is about one order larger than that by the one-loop $gg\to W^{\pm}H^{\mp}$. Of course the consideration ignoring the squark loops in subprocess $gg\to W^{\pm}H^{\mp}$ is reasonable when the masses of supersymmetric particles are very heavy, and it leads to the cross-section contributions from squark loops being very small due to the decoupling theorem. But in the

MSSM theory the nondecoupling squark masses are also possible, thereby the effects from the squark loop diagrams could be important. Recently, Yang *et al.* calculated the supersymmetric electroweak corrections to $b\bar{b}\to W^{\pm}H^{\mp}$ at the LHC [16].

In this paper we give the calculation of the process $pp\to gg+X\to W^{\pm}H^{\mp}+X$ at the CERN LHC including the contributions, which arise from both quark and squark loop diagrams in the framework of the MSSM. We arrange this paper as follows. In Sec. II we present the analytical calculation. In Sec. III we give some numerical presentations including the results from the input parameters of the minimal supergravity (MSUGRA) scenario [17], and discuss these numerical results. The conclusions are contained in Sec. IV. Finally, some notations used in this paper and the explicit expressions of the relevant form factors induced by the loop diagrams are collected in the Appendix.

II. THE CALCULATION OF $pp\to gg\to W^+H^-+X$

In the MSSM theory every quark has two scalar partners, the squarks $\tilde{q}_L$ and $\tilde{q}_R$. If there is no left-right flavor mixing in the squark-sector, the mass matrix of a scalar quark including CP-odd phases takes the following form [18]:

$$-\mathcal{L}_m=(\tilde{q}_L^* \quad \tilde{q}_R^*)\begin{pmatrix} m^2_{\tilde{q}_L} & a_q m_q \\ a_q^* m_q & m^2_{\tilde{q}_R}\end{pmatrix}\begin{pmatrix}\tilde{q}_L \\ \tilde{q}_R\end{pmatrix}, \tag{2.1}$$

where $\tilde{q}_L$ and $\tilde{q}_R$ are the current eigenstates. For the up-type scalar quarks, we have

$$m^2_{\tilde{q}_L}=\tilde{M}_Q^2+m_q^2+m_Z^2\left(\frac{1}{2}-Q_q s_W^2\right)\cos 2\beta, \tag{2.2}$$

$$m^2_{\tilde{q}_R}=\tilde{M}_U^2+m_q^2+Q_q m_Z^2 s_W^2\cos 2\beta, \tag{2.3}$$

$$a_q=|a_q|e^{-2i\phi_q}=\mu\cot\beta+A_q^*\tilde{M}. \tag{2.4}$$

For the down-type scalar quarks,

$$m^2_{\tilde{q}_L}=\tilde{M}_Q^2+m_q^2-m_Z^2\left(\frac{1}{2}+Q_q s_W^2\right)\cos 2\beta, \tag{2.5}$$

$$m^2_{\tilde{q}_R}=\tilde{M}_D^2+m_q^2+Q_q m_Z^2 s_W^2\cos 2\beta, \tag{2.6}$$

$$a_q=|a_q|e^{-2i\phi_q}=\mu\tan\beta+A_q^*\tilde{M}, \tag{2.7}$$

where Q_q ($Q_D=-\frac{1}{3}$, $Q_U=\frac{2}{3}$) is the charge of the scalar quark, $\tilde{M}_Q^2$, $\tilde{M}_U^2$, and $\tilde{M}_D^2$ are the self-supersymmetry-breaking mass terms for the left-handed and right-handed scalar quarks, and $s_W=\sin\theta_W$, $c_W=\sin\theta_W$. We choose $\tilde{M}_Q=\tilde{M}_U=\tilde{M}_D=\tilde{M}$. $A_q\cdot\tilde{M}$ is a trilinear scalar interaction parameter, and μ is the supersymmetric mass mixing term of the Higgs boson. The complex value a_q can introduce CP violation. In general, $\tilde{q}_L$ and $\tilde{q}_R$ are mixed and give the mass eigenstates $\tilde{q}_1$ and $\tilde{q}_2$ (usually we assume $m_{\tilde{q}_1}<m_{\tilde{q}_2}$). The mass eigenstates $\tilde{q}_1$ and $\tilde{q}_2$ are expressed in terms of the current eigenstates $\tilde{q}_L,\tilde{q}_R$ and the mixing angle θ_q with the CP-violating phase ϕ_q. They read

$$\tilde{q}_1=\tilde{q}_L\cos\theta_q e^{i\phi_q}-\tilde{q}_R\sin\theta_q e^{-i\phi_q},$$

$$\tilde{q}_2=\tilde{q}_L\sin\theta_q e^{i\phi_q}+\tilde{q}_R\cos\theta_q e^{-i\phi_q}, \tag{2.8}$$

and

$$\tan 2\theta_q=\frac{2|a_q|m_q}{m^2_{\tilde{q}_L}-m^2_{\tilde{q}_R}}. \tag{2.9}$$

Then the masses of $\tilde{q}_1$ and $\tilde{q}_2$ are

$$(m^2_{\tilde{q}_1},m^2_{\tilde{q}_2})=\frac{1}{2}\{m^2_{\tilde{q}_L}+m^2_{\tilde{q}_R}\mp[(m^2_{\tilde{q}_L}-m^2_{\tilde{q}_R})^2+4|a_q|^2m_q^2]^{1/2}\}. \tag{2.10}$$

In this work we ignore the CP violation and take all those CP-violating phases being zero. In this case the cross section of $pp\to gg+X\to W^-H^+X$ coincides with the process $pp\to gg+X\to W^+H^-+X$ because of charge conjugation invariance. We are now ready to calculate the process $pp\to gg+X\to W^+H^-+X$. Unless otherwise stated, the calculation in Sec. II is specified in this process only, whereas numerical results of the total cross section in Sec. III involve both processes, i.e., $pp\to gg+X\to W^{\pm}H^{\mp}+X$. Hence our numerical results of total cross section contain a factor of 2 in contrast to W^+H^- production only.

In our calculation, we perform the calculation in the 't Hooft-Feynman gauge. As the subprocess $gg\to W^+H^-$ is loop-induced, the one-loop order calculation can be simply carried out by summing all unrenormalized reducible and irreducible one-loop diagrams and the results will be finite and gauge invariant. The generic Feynman diagrams contributing to the subprocess in the MSSM at one-loop level are depicted in Fig. 1, where the exchange of incoming gluons in Fig. 1(a.1–4), Fig. 1(b.2), and Fig. 1 (c.1 and 2) are not shown. In Fig. 1, $U(\tilde{U})=u,c,t(\tilde{u},\tilde{c},\tilde{t})$, $D(\tilde{D})=d,s,b(\tilde{d},\tilde{s},\tilde{b})$. We found that diagrams like Fig. 1(b.2) do not contribute to the cross section and are thus excluded in the form factor expressions in the Appendix. In our numerical evaluation we consider only the contributions from the third generation quarks and squarks, i.e., $U(\tilde{U})=t(\tilde{t})$, $D(\tilde{D})=b(\tilde{b})$, due to the feature of the Yukawa coupling strength.

We divide all the one-loop diagrams in Fig. 1 into three groups: (1) box diagrams shown in Fig. 1(a.1–4), (2) quartic interaction diagrams in Fig. 1(b.1–3), (3) triangle diagrams shown in Fig. 1(c.1 and 2). We denote the reaction of W^+H^- production via gluon-gluon fusion as

$$g(p_1,\alpha,\mu)g(p_2,\beta,\nu)\to W^+(k_1,\lambda)H^-(k_2). \tag{2.11}$$

where p_1,p_2 and k_1,k_2 denote the four momenta of the incoming gluons and outgoing W^+ and H^-, respectively,

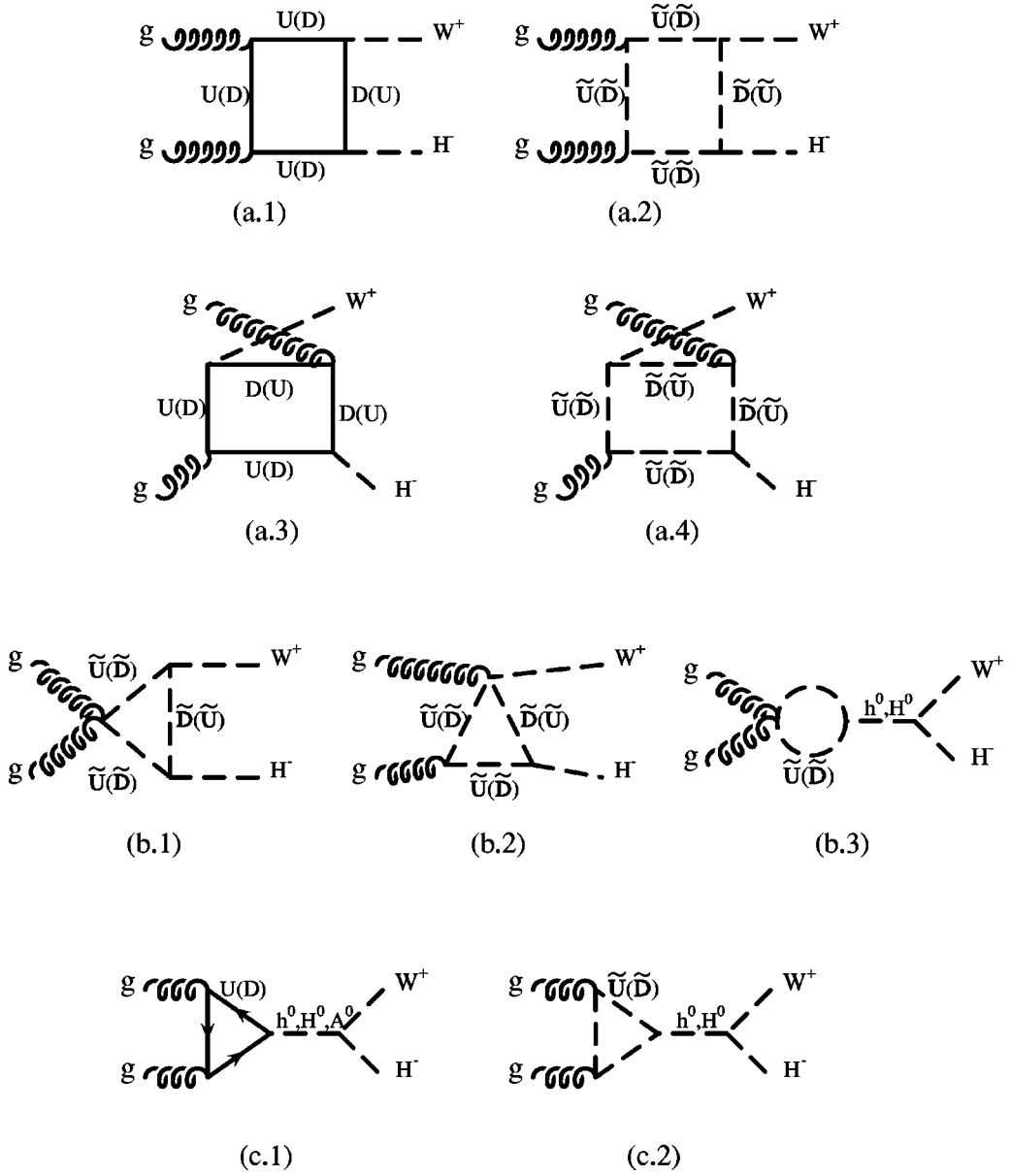

FIG. 1. The Feynman diagrams of the subprocess $gg \to W^+H^-$. (a.1–4) Box diagrams. (b.1–3) quartic interaction diagrams. (c.1 and 2) Triangle diagrams.

while α,β are color indices of the colliding gluons. The Mandelstam variables are defined as

$$\hat{s}=(p_1+p_2)^2=(k_1+k_2)^2, \quad \hat{t}=(p_1-k_1)^2=(p_2-k_2)^2,$$

$$\hat{u}=(p_1-k_2)^2=(p_2-k_1)^2. \tag{2.12}$$

The explicit expression of the corresponding matrix element can be found in the Appendix. The parton level cross section at one-loop order with summing all the spins of final states and averaging the spin and color of initial states can be obtained from

$$\hat{\sigma}(\hat{s},gg\to W^+H^-)=\frac{1}{16\pi\hat{s}^2}\int_{\hat{t}^-}^{\hat{t}^+} d\hat{t}\ \ \overline{\sum}\ |\mathcal{M}|^2. \tag{2.13}$$

In the above equation, we take $\hat{t}^{\pm}=[(m_H^2+m_W^2-\hat{s}) \pm \sqrt{(m_H^2+m_W^2-\hat{s})^2-4m_H^2m_W^2}]/2$. The bar over the sum means the average over the initial spin and color. It leads to the color factor in the cross section which is equal to 1/32 and arises from

$$\frac{1}{8}\frac{1}{8}\sum_{\alpha,\beta}[\mathrm{tr}(T_\alpha T_\beta)]^2=\frac{1}{8}\frac{1}{8}\frac{1}{4}8=\frac{1}{32}. \tag{2.14}$$

The total cross section of the W^+H^- production via gluon fusion at hadron collider can be obtained by folding the cross section of the subprocess $\hat{\sigma}(gg\to W^+H^-)$ with the gluon-gluon luminosity.

$$\sigma(s,pp\to gg\to W^+H^-)$$
$$=\int_{\frac{m_{W^+}+m_{H^+}}{\sqrt{s}}}^{1} dz\frac{dL_{gg}}{dz}\hat{\sigma}(gg\to W^+H^- \quad \text{at} \quad \hat{s}=z^2s), \tag{2.15}$$

where $\sqrt{s}$ and $\sqrt{\hat{s}}$ are the pp and gg c.m.s. energies, respectively, and $d\mathcal{L}_{gg}/dz$ is the gluon-gluon luminosity at proton-proton collider, which is expressed as [20]

$$\frac{d\mathcal{L}_{gg}}{dz}=\frac{1}{2}\int_z^1\frac{dx_1}{x_1}\left[f_g(x_1,Q)f_g\left(\frac{z}{x_1},Q\right)+f_g\left(\frac{z}{x_1},Q\right)f_g(x_1,Q)\right]. \tag{2.16}$$

The differential cross section for $pp\to gg\to W^+H^-+X$ is conveniently written in terms of the rapidities y_1 and y_2 of the two jets (finial states) and W-boson transverse momentum p_T. Here we neglect the intrinsic transverse momentum carried by partons. It is

$$\frac{d\sigma}{dy_1dy_2dp_T}=\frac{\pi z^2p_T}{\hat{s}}f_g(x_1,Q)f_g(x_2,Q)\times\hat{\sigma}(gg\to W^+H^- \quad \text{at} \quad \hat{s}=z^2s), \tag{2.17}$$

$f_g(x_i,\mu)$ is the distribution function of gluon in proton. Defining

$$y^*=\frac{1}{2}(y_1-y_2), \quad y_{boost}=\frac{1}{2}(y_1+y_2). \tag{2.18}$$

We may write

$$z^2=\frac{4p_T^2}{s}\cosh^2 y^* \tag{2.19}$$

$$x_1=ze^{y_{boost}}, \quad x_2=ze^{-y_{boost}}. \tag{2.20}$$

III. NUMERICAL RESULTS AND DISCUSSIONS

In this section, we present some numerical results of the total cross section from the quark and squark one-loop diagrams for the processes $pp\to gg+X\to W^\pm H^\mp+X$. The SM input parameters are chosen as $m_t=175$ GeV, $m_Z=91.187$ GeV, $m_b=4.5$ GeV, $\sin^2\theta_W=0.2315$, and $\alpha_{EW}=1/128$ [19]. We adopt CTEQ5 of the parton distribution functions proton (set 1) [21] in integrating the parton level cross section, and take the renormalization scale and factorization scale to be the identical value of $\mu=Q=m_W+m_{H^+}$. We adopt a simple one-loop formula for the running strong coupling α_s as

$$\alpha_s(\mu)=\frac{\alpha_s(m_Z)}{1+\frac{33-2n_f}{6\pi}\alpha_s(m_Z)\ln\left(\frac{\mu}{m_Z}\right)}, \tag{3.1}$$

TABLE I. The squark masses with input parameters $\tilde{M}=220$ GeV, $\mu=300$ GeV, and mixing angles $\theta_{\tilde{b}}=0$, $\theta_{\tilde{t}}=\pi/4$.

$\tan\beta$	$m_{\tilde{b}_1}$	$m_{\tilde{b}_2}$	$m_{\tilde{t}_1}$	$m_{\tilde{t}_2}$
1.5	220.593 GeV	223.111 GeV	240.846 GeV	313.758 GeV
6	221.389 GeV	227.509 GeV	165.324 GeV	356.069 GeV
30	221.462 GeV	227.911 GeV	156.523 GeV	359.725 GeV

where $\alpha_s(m_Z)=0.117$ and n_f is the number of active flavors at energy scale μ.

The supersymmetric input parameter sector is given in two ways. First, we run the package HDECAY [22] in the MSSM mode by choosing $\tan\beta$ (ratio of the vacuum expectation values of the two Higgs fields) and m_{H^+} (pole mass of the charged Higgs boson) as the input parameters of the Higgs sector, we obtain the masses of the neutral Higgs boson, $(m_{h^0},m_{H^0},m_{A^0})$, decay widths $\Gamma_{h^0},\Gamma_{H^0},\Gamma_{A^0}$, as well as the mixing angle (α) of the neutral Higgs bosons h^0 and H^0. In fact, our input value of $\tan\beta$ varies in the range of 1.5–32, and m_{H^+} from 100 to 1000 GeV. For the scalar quark sector, we choose the supersymmetric mass parameter of the Higgs boson and self-supersymmetry-breaking mass $\tilde{M}$ as $\mu=300$ GeV and $\tilde{M}=220$ GeV and take the mixing angles $\theta_{\tilde{b}}=0$ and $\theta_{\tilde{t}}\sim\pi/4$, so that the masses of top squark pair split remarkably, while the split of the bottom squark masses is minimized. With the input parameters mentioned above, the masses of scalar quarks can be obtained from Eqs. (2.2)–(2.10). We list them in Table I.

The cross sections for the subprocess $gg\to W^+H^-$ versus gluon-gluon c.m.s. energy $\sqrt{\hat{s}}$ is shown in Fig. 2. The input parameters are set to typical values of $\tan\beta=1.5$, 6, and 30, while $m_{H^+}=150$ and 600 GeV, respectively. There are some peaks on the curves which reflect the resonance effects in top quark and top squark/bottom squark loops, respectively. For instance, let us look at the dashed line ($\tan\beta$

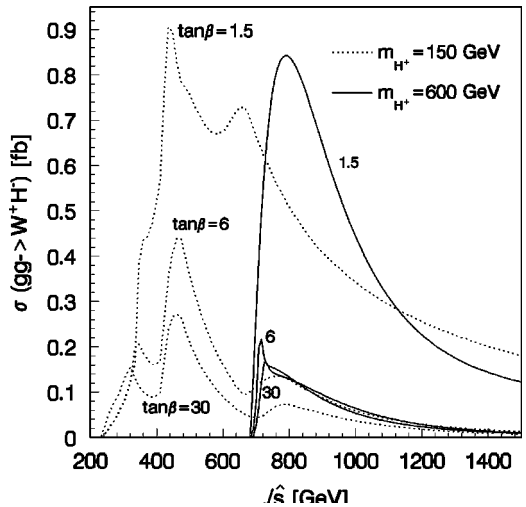

FIG. 2. Cross sections of the subprocess $gg\to W^+H^-$ as function of gg c.m.s energy $\sqrt{\hat{s}}$. Note that W^-H^+ production rate is not counted here.

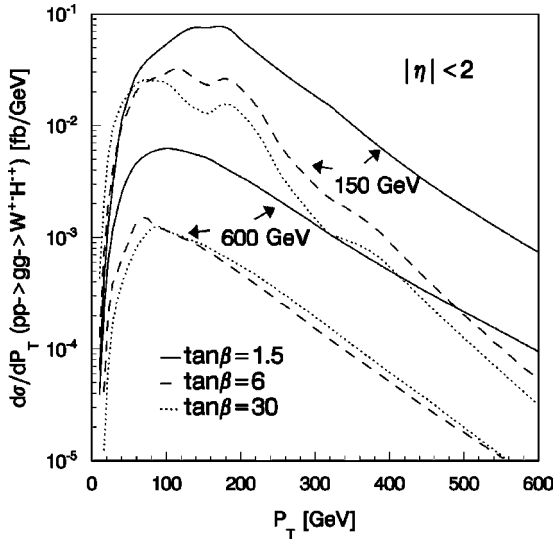

FIG. 3. Transverse momentum spectrum $d\sigma/dp_T$ of $pp \to gg + X \to W^{\pm}H^{\mp} + X$ at LHC with $\sqrt{s} = 14$ TeV and the cut of pseudorapidity $|\eta| < 2$. The upper three curves are for $m_{H^+} = 150$ GeV, $\tan\beta = 1.5,6,30$ respectively. The other three curves are for $m_{H^+} = 600$ GeV.

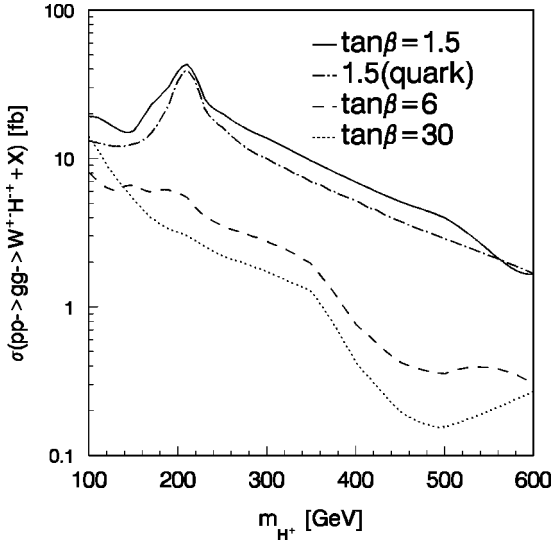

FIG. 4. Total cross sections of the process $pp \to gg + X \to W^{\pm}H^{\mp} + X$ as function of m_{H^+} at LHC with $\sqrt{s} = 14$ TeV. The curve labeled ''quark'' denotes the contribution from quark loops only.

$= 6$, $m_{H^+} = 150$ GeV). The obvious peaks at the vicinities of $\sqrt{\hat{s}} = 2m_{\tilde{q}_{1,2}}$ ($\tilde{q} = \tilde{t}, \tilde{b}$) are from the enhancement by the resonance effects of the $\tilde{t}_1$ loop together with the top quark loop, $\tilde{b}_{1,2}$, $\tilde{t}_2$ loop diagrams, respectively. For $m_{H^+} = 600$ GeV, the only kinematically allowed sharp peak at $\sqrt{\hat{s}} = 2m_{\tilde{t}_2}$ is from the $\tilde{t}_2$ resonance effect.

The p_T distributions $d\sigma/dp_T$ with $\sqrt{s} = 14$ TeV is shown in Fig. 3 with the cut of pseudorapidity $|\eta| < 2$. Again the six curves correspond to the parameter sets of $\tan\beta = 1.5$, 6, 30, and $m_{H^+} = 150$ and 600 GeV, respectively. Because of the contributions from the scalar quark loop diagrams, the p_T distributions have some structures at the regions when $p_T \sim 380$ GeV and $p_T \sim 180$ GeV, on the curves for $m_{H^+} = 150$ GeV with $\tan\beta = 6,30$, respectively. The curves for $m_{H^+} = 150$ GeV with $\tan\beta = 1.5$ has a small peak at about $p_T \sim 180$ GeV only. For the curves of $m_{H^+} = 600$ GeV, there is no obvious structure on their line shapes.

Figure 4 displays the integrated total cross section of $W^{\pm}H^{\mp}$ production at proton-proton colliders versus the mass of $H^{\pm}$ with $\sqrt{s} = 14$ TeV. There we can see the sophisticated structures on all curves. For comparison we plot the curve for $\tan\beta = 1.5$ with only quark loop contributions too. We can see that the cross sections are enhanced by the scalar quark loop contributions. The increment can reach 70% comparing with the cross section with only quark loop diagrams. In Fig. 4, all these structures come also from the contributions of threshold effects at the vicinities where $m_{H^+} = m_{\tilde{t}_i} + m_{\tilde{b}_i}$ $(i = 1,2)$ and $m_{H^+} = m_t + m_b$ from loop diagrams. At some of these positions the threshold effects are not so obvious for the parent process. When $\tan\beta = 1.5$, the cross section could reach up to 45 fb in the vicinity of $m_{H^+} \sim 210$ GeV. Note that the heavy scalar quark $\tilde{t}_i$ and $\tilde{b}_i$ $(i = 1,2)$ in loops could slightly increase the cross section at large charged Higgs boson mass region of approximately $m_{\tilde{b}_1} + m_{\tilde{t}_1} \sim 460$ GeV to $m_{\tilde{b}_2} + m_{\tilde{t}_2} \sim 540$ GeV, due to top squark–bottom squark loop diagrams Figs. 1(a.2), 1(a.4), and 1(b.1).

In Fig. 5 we present the cross sections of $W^{\pm}H^{\mp}$ productions versus $\tan\beta$ with $\sqrt{s} = 14$ TeV and the mass of the charged Higgs boson is chosen as 100, 300, and 1000 GeV, respectively. Our calculation shows that since the couplings of Higgs bosons to quark or squark pairs are related to the ratio of the vacuum expectation values, $\tan\beta$ should effect the cross sections substantially. When the ratio of both vacuum expectation values $\tan\beta$ is in the low value range, the cross sections for those three curves can reach their maximum values.

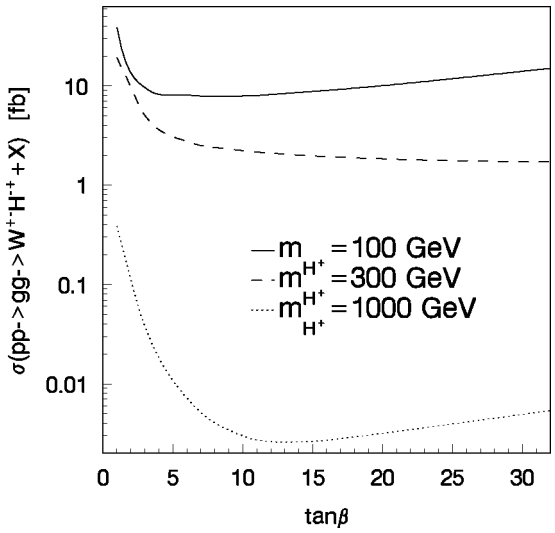

FIG. 5. Total cross sections of the process $pp \to gg + X \to W^{\pm}H^{\mp} + X$ as function of $\tan\beta$ at LHC with $\sqrt{s} = 14$ TeV.

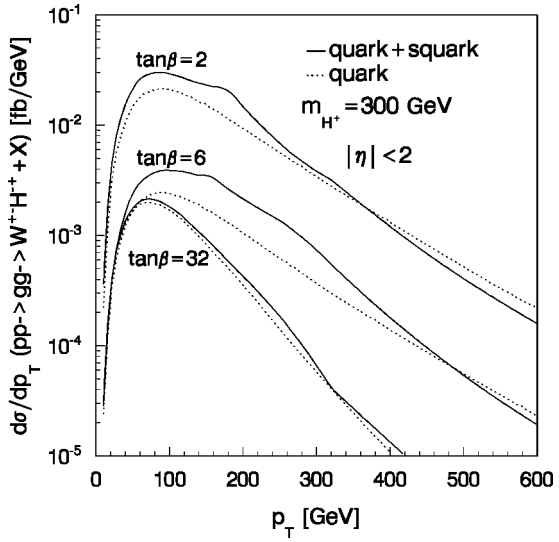

FIG. 6. Transverse momentum spectrum $d\sigma/dp_T$ in the MSUGRA scenario of $pp \to gg+X \to W^{\pm}H^{\mp}+X$ at LHC with $\sqrt{s}=14$ TeV and the cut of pseudorapidity $|\eta|<2$. The three curves are for $m_{H^+}=300$ GeV, $\tan\beta=2,6,32$ respectively.

Figures 6, 7, and 8, which correspond to Figs. 2, 3, and 5, respectively, are worked out in the MSUGRA scenario. Of the five input parameters (m_0, $m_{1/2}$, A_0, $\tan\beta$, and sign of μ) in this theory, we take $m_{1/2}=120$ GeV, $A_0=300$ GeV, $\mu>0$. m_0 is obtained from the chosen values of $m_{H^{\pm}}$. All other MSSM parameters are determined in the MSUGRA scenario by using program package ISAJET 7.44. In this program, the renormalization group equations (RGE's) [23] are run from the weak scale m_Z up to the grand unified theory (GUT) scale, taking all thresholds into account in order to get the low-energy scenario from the MSUGRA. It uses two-loop RGE's only for the gauge couplings and the one-loop RGE's for the other supersymmetric parameters. The GUT scale boundary conditions are imposed and the RGE's are

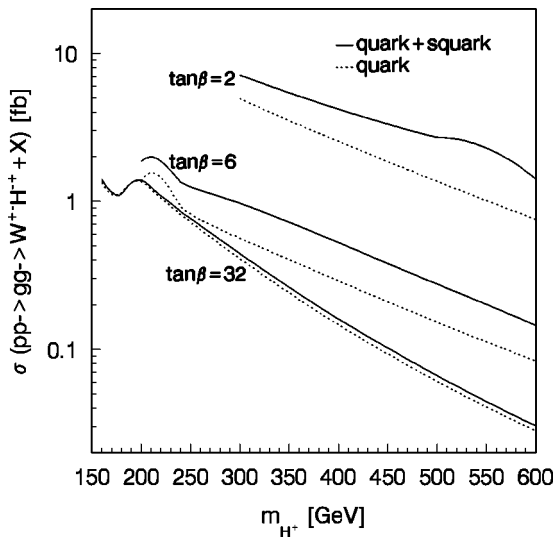

FIG. 7. Total cross sections in MSUGRA scenario as function of $m_{H^{\pm}}$ at LHC with $\sqrt{s}=14$ TeV. Dotted curves denote the contribution from quark loops only.

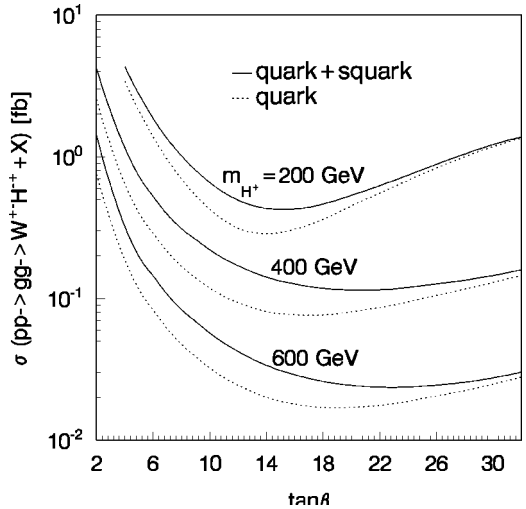

FIG. 8. Total cross sections in MSUGRA scenario as function of $\tan\beta$ at LHC with $\sqrt{s}=14$ TeV. Dotted curves denote the contribution from quark loops only.

run back to m_Z, again taking threshold into account. In these figures we plot the curves contributed by (s)quark loops and only quark loop diagrams separately for comparison. All three figures show that the cross sections are effected by the supersymmetric contributions obviously. In Fig. 6, we find that scalar quark corrections can be either positive or negative. When the value of *W*-boson transverse momentum p_T is getting rather large, the scalar quark contribution is becoming negative. The supersymmetric correction to the transverse momentum distribution can be more than 80% of the total momentum distribution. Figures 7 and 8 show that the squark loop correction increases with the increment of the charged Higgs mass, and decreases with the increment of $\tan\beta$ in the region of $\tan\beta>10$. It exceeds $+50\%$ of the total cross section for small $\tan\beta$ and large charged Higgs mass. Even when $\tan\beta=2$ and $m_{H^{\pm}}=550$ GeV, the supersymmetric correction reaches $+56\%$. Compared with previous figures with non-MSUGRA parameters, we observe less obvious scalar-quark contributions in some parameter space, which is partly suppressed due to decoupling scalar-quark masses and partly due to constraints to scalar quark coupling strength.

In order to check our calculation, the comparisons of our results with those reported in Refs. [13] and [14] are made, respectively. With the same input parameters as in Ref. [13] and ignoring the squark loop contributions, we can reproduce the results of theirs very well, while if we use the input information from Ref. [14] and assume having a decoupling scalar quark interaction, our cross sections are exactly one half of their corresponding values in Ref. [14]. During the revision of our manuscript, we acknowledged another paper which appeared on this subject [24]. We made further comparison with the results in this paper. Our calculation shows that if we use their input parameters, we get again exactly one half of their corresponding values in Ref. [24].

IV. SUMMARY

In this paper, we studied the $W^{\pm}$-associated production of charged Higgs bosons via gluon-gluon fusion in the MSSM

at the LHC. Numerical analysis of their production rates is carried out at (s)quark one-loop order with some typical parameter sets. With our input parameters the contribution from virtual scalar quarks are obvious in most parameter space regions and cannot be neglected. We find the contributions from the scalar quark loops are comparable with that from quark loop diagrams and can either decrease or enhance the cross section substantially. In the MSUGRA scenario, the squark loop contribution can even reach $+56\%$ of the total cross section. Our results demonstrate that this cross section can be about 45 fb with our chosen input parameters at the CERN LHC. The analysis of the p_T distribution shows that its line shapes depend partly on the virtual scalar quark contributions.

ACKNOWLEDGMENTS

This work was supported in part by the National Natural Science Foundation of China (Project No. 19875049), the Youth Science Foundation of the University of Science and Technology of China, a grant from the Education Ministry of China and the State Commission of Science and Technology of China. The authors would like to thank Professor Edmond L. Berger for helpful discussion.

APPENDIX

In this appendix we list the form factors for the one-loop diagrams of the third generation quarks and squarks. The notations used in this section are defined as below:

$$P_A=\frac{1}{\hat{s}-{m_{A^0}}^2+im_{A^0}\Gamma_{A^0}},$$

$$P_h=\frac{1}{\hat{s}-{m_{h^0}}^2+im_{h^0}\Gamma_{h^0}},\quad P_H=\frac{1}{\hat{s}-{m_{A^0}}^2+im_{H^0}\Gamma_{H^0}},$$

$$P_b=P_h\cos(\alpha-\beta)\sin\alpha-P_H\sin(\alpha-\beta)\cos\alpha,$$

$$P_t=P_h\cos(\alpha-\beta)\cos\alpha+P_H\sin(\alpha-\beta)\sin\alpha,$$

$$B_0^t=B_0[-p_1,m_t,m_t],\quad B_0^b=B_0[-p_1,m_b,m_b],$$

$$B_0^{\tilde{t}}=B_0[p_1+p_2,m_{\tilde{t}x},m_{\tilde{t}x}],$$

$$B_0^{\tilde{b}}=B_0[p_1+p_2,m_{\tilde{b}x},m_{\tilde{b}x}],$$

$$C_{ij}^t=C_{ij}[-p_2,-p_1,m_t,m_t,m_t],$$

$$C_{ij}^b=C_{ij}[-p_2,-p_1,m_b,m_b,m_b],$$

$$C_{ij}^{\tilde{t}}=C_{ij}[-p_2,-p_1,m_{\tilde{t}x},m_{\tilde{t}x},m_{\tilde{t}x}],$$

$$C_{ij}^{\tilde{b}}=C_{ij}[-p_2,-p_1,m_{\tilde{b}x},m_{\tilde{b}x},m_{\tilde{b}x}],$$

$$C_{ij}^1=C_{ij}[k_2,k_1,m_{\tilde{t}y},m_{\tilde{b}x},m_{\tilde{t}y}],$$

$$C_{ij}^2=C_{ij}[k_2,k_1,m_{\tilde{b}y},m_{\tilde{t}x},m_{\tilde{b}y}],$$

$$C_{ij}^3=C_{ij}[k_2,-p_2,m_{\tilde{t}y},m_{\tilde{b}x},m_{\tilde{b}x}],$$

$$C_{ij}^4=C_{ij}[k_2,-p_2,m_{\tilde{b}y},m_{\tilde{t}x},m_{\tilde{t}x}],$$

$$C_{ij}^5=C_{ij}[k_2,-p_1,m_{\tilde{t}y},m_{\tilde{b}x},m_{\tilde{b}x}],$$

$$C_{ij}^6=C_{ij}[k_2,-p_1,m_{\tilde{b}y},m_{\tilde{t}x},m_{\tilde{t}x}],$$

$$V_{h\tilde{t}_x\tilde{t}_y}=i\left[\frac{m_Z}{c_W}\left(\frac{1}{2}-\frac{2}{3}s_W^2\right)\sin(\alpha+\beta)-\frac{m_t^2}{m_W\sin\beta}\cos\alpha\right]U_{1i}^*U_{1j}+i\left[\frac{2m_Z}{3c_W}s_W^2\sin(\alpha+\beta)-\frac{m_t^2}{m_W\sin\beta}\cos\alpha\right]U_{2i}^*U_{2j}+i\frac{m_t}{2m_W\sin\beta}\times(-A_t\cos\alpha+\mu\sin\alpha)(U_{2i}^*U_{1j}+U_{1i}^*U_{2j}),$$

$$V_{H\tilde{t}_x\tilde{t}_y}=-i\left[\frac{m_Z}{c_W}\left(\frac{1}{2}-\frac{2}{3}s_W^2\right)\cos(\alpha+\beta)+\frac{m_t^2}{m_W\sin\beta}\sin\alpha\right]U_{1i}^*U_{1j}-i\left[\frac{2m_Z}{3c_W}s_W^2\cos(\alpha+\beta)+\frac{m_t^2}{m_W\sin\beta}\sin\alpha\right]U_{2i}^*U_{2j}-i\frac{m_t}{2m_W\sin\beta}\times(A_t\sin\alpha+\mu\cos\alpha)(U_{2i}^*U_{1j}+U_{1i}^*U_{2j}),$$

$$V_{h\tilde{b}_x\tilde{b}_y}=i\left[-\frac{m_Z}{c_W}\left(\frac{1}{2}-\frac{1}{3}s_W^2\right)\sin(\alpha+\beta)+\frac{m_b^2}{m_W\cos\beta}\sin\alpha\right]D_{1i}^*D_{1j}+i\left[-\frac{m_Z}{3c_W}s_W^2\sin(\alpha+\beta)+\frac{m_b^2}{m_W\cos\beta}\sin\alpha\right]\times D_{2i}^*D_{2j}-i\frac{m_b}{2m_W\cos\beta}(-A_b\sin\alpha+\mu\cos\alpha)\times(D_{2i}^*D_{1j}+D_{1i}^*D_{2j}),$$

$$V_{H\tilde{b}_x\tilde{b}_y}=i\left[\frac{m_Z}{c_W}\left(\frac{1}{2}-\frac{1}{3}s_W^2\right)\cos(\alpha+\beta)-\frac{m_b^2}{m_W\cos\beta}\cos\alpha\right]D_{1i}^*D_{1j}-i\left[-\frac{m_Z}{3c_W}s_W^2\cos(\alpha+\beta)+\frac{m_b^2}{m_W\cos\beta}\cos\alpha\right]\times D_{2i}^*D_{2j}-i\frac{m_b}{2m_W\cos\beta}(A_b\cos\alpha+\mu\sin\alpha)\times(D_{2i}^*D_{1j}+D_{1i}^*D_{2j}),$$

$$V_{H\tilde{t}_x\tilde{b}_y}=-i\frac{m_W}{\sqrt{2}}[\sin 2\beta-(m_b^2\tan\beta+m_t^2\cot\beta)/m_W^2]U_{1i}^*D_{1j}+i\frac{m_tm_b}{\sqrt{2}m_W}\times(\tan\beta+\cot\beta)U_{2i}^*D_{2j}-i\frac{m_b}{\sqrt{2}m_W}\times(\mu-A_b\tan\beta)U_{1i}^*D_{2j}-i\frac{m_t}{\sqrt{2}m_W}\times(\mu-A_t\cot\beta)U_{2i}^*D_{1j},$$

$$V_{W\tilde{t}_x\tilde{b}_y}=-iD_{1x}^*U_{1y}/\sqrt{2},$$

$$F_1[f(x,y)]=4m_W\sum_{x,y=1}^{2}f(x,y)V_{H\tilde{t}_x\tilde{b}_y}V_{W\tilde{b}_y\tilde{t}_x},$$

$$F_2[f(x,y)]=4m_W\sum_{x,y=1}^{2}f(x,y)V_{H\tilde{t}_y\tilde{b}_x}V_{W\tilde{b}_x\tilde{t}_y},$$

where the indices $x,y(=1,2)$ of U and D label squark mass eigenstates. The elements of the transform matrix between squark current eigenstates and mass eigenstates Q_{xy} $(Q=U,D)$ are defined as

$$Q=\begin{pmatrix}\cos\theta_q e^{-i\phi_q} & \sin\theta_q e^{-i\phi_q}\\ -\sin\theta_q e^{i\phi_q} & \cos\theta_q e^{i\phi_q}\end{pmatrix}.$$

The matrix element corresponding to Fig. 1 can be written as

$$\mathcal{M}=\mathcal{M}_b+\mathcal{M}_q+\mathcal{M}_s,$$

where the contribution of the s-channel [Fig. 1(b.3), (c.1 and 2)] to the matrix element is

$$\mathcal{M}_s=\frac{i\delta_{\alpha\beta}\epsilon^{\mu}(p_1)\epsilon^{\nu}(p_2)\epsilon^{\lambda}(-k_1)g_s^2g_e^2}{16\pi^2m_W}(p_1+p_2)_\lambda\{f_1^s\epsilon_{\mu\nu p_1p_2}+f_2^sp_{2\mu}p_{1\nu}+f_3^sg_{\mu\nu}\}.$$

The contribution of quartic diagrams Fig. 1(b1 and 2) to the matrix element is

$$\mathcal{M}_q=\frac{i\delta_{\alpha\beta}\epsilon^{\mu}(p_1)\epsilon^{\nu}(p_2)\epsilon^{\lambda}(-k_1)g_s^2g_e^2}{16\pi^2m_W}f_3^q(p_1+p_2)_\lambda g_{\mu\nu}.$$

The form factors f_i $(i=1-5)$ are expressed explicitly as follows. g_s represents the coupling constant for the strong interation and g_e for electroweak interactions:

$$f_1^s=-2iP_A(m_t^2\cot\beta C_0^t+m_b^2\tan\beta C_0^b),$$

$$f_2^s=-2P_tm_t^2\csc\beta(C_0^t+4C_{12}^t+4C_{23}^t)+2P_bm_b^2\times\sec\beta(C_0^b+4C_{12}^b+4C_{23}^b)+4im_W\times\sum_{x=1}^{2}[P_h\cos(\alpha-\beta)V_{h\tilde{t}_x\tilde{t}_x}+P_H\sin(\alpha-\beta)V_{H\tilde{t}_x\tilde{t}_x}](C_{12}^{\tilde{t}}+C_{23}^{\tilde{t}})+[P_h\cos(\alpha-\beta)V_{h\tilde{b}_x\tilde{b}_x}+P_H\sin(\alpha-\beta)V_{H\tilde{b}_x\tilde{b}_x}]\times(C_{12}^{\tilde{b}}+C_{23}^{\tilde{b}}),$$

$$f_3^s=-2P_tm_t^2\csc\beta\left(B_0^t-\frac{\hat{s}}{2}C_0^t-\hat{s}C_{12}^t-4C_{24}^t\right)+2P_bm_b^2\sec\beta\left(B_0^b-\frac{\hat{s}}{2}C_0^b-\hat{s}C_{12}^b-4C_{24}^b\right)+im_W\sum_{x=1}^{2}[P_h\cos(\alpha-\beta)V_{h\tilde{t}_x\tilde{t}_x}+P_H\sin(\alpha-\beta)V_{H\tilde{t}_x\tilde{t}_x}]\times(B_0^{\tilde{t}}-4C_{24}^{\tilde{t}})+[P_h\cos(\alpha-\beta)V_{h\tilde{b}_x\tilde{b}_x}+P_H\times\sin(\alpha-\beta)V_{H\tilde{b}_x\tilde{b}_x}](B_0^{\tilde{b}}-4C_{24}^{\tilde{b}}),$$

$$f_3^q=\frac{1}{2}F_1[C_0^2+C_{11}^2]-\frac{1}{2}F_2[C_0^1+C_{11}^1].$$

For box diagrams [Fig. 1(a.1–4)], we define the following notations:

$$D_{ij}^{b1}=D_{ij}[k_1,-p_2,-p_1,m_t,m_b,m_b,m_b],$$

$$C_{ij}^{b1}=C_{ij}[-p_2,-p_1,m_b,m_b,m_b],$$

$$D_{ij}^{b3}=D_{ij}[k_1,-p_1,-p_2,m_t,m_b,m_b,m_b],$$

$$C_{ij}^{b3}=C_{ij}[-p_1,-p_2,m_b,m_b,m_b],$$

$$D_{ij}^{b5}=D_{ij}[-p_2,k_1,-p_1,m_t,m_t,m_b,m_b],$$

$$C_{ij}^{b5}=C_{ij}[k_1,-p_1,m_t,m_b,m_b],$$

$$D_{ij}^{bk}=D_{ij}^{b(k-1)}(t\leftrightarrow b),\quad C_{ij}^{bk}=C_{ij}^{b(k-1)}(t\leftrightarrow b),\quad (k=2,4,6)$$

$$D_{ij}^{s1}=D_{ij}[k_1,-p_2,-p_1,m_{\tilde{t}y},m_{\tilde{b}x},m_{\tilde{b}x},m_{\tilde{b}x}],$$

$$D_{ij}^{s3}=D_{ij}[k_1,-p_1,-p_2,m_{\tilde{t}y},m_{\tilde{b}x},m_{\tilde{b}x},m_{\tilde{b}x}],$$

$$D_{ij}^{s5}=D_{ij}[-p_2,k_1,-p_1,m_{\tilde{t}y},m_{\tilde{t}y},m_{\tilde{b}x},m_{\tilde{b}x}],$$

$$D_{ij}^{sk}=D_{ij}^{s(k-1)}(\tilde{t}\leftrightarrow\tilde{b}),\quad (k=2,4,6)$$

$$T_t=m_t^2\tan\beta.$$

With replacement between t channel and u channel, the contribution from box diagrams is

$$\mathcal{M}_b=\frac{i\delta_{\alpha\beta}\epsilon^{\mu}(p_1)\epsilon^{\nu}(p_2)\epsilon^{\lambda}(-k_1)g_s^2g_e^2}{16\pi^2m_W}\{g_1g_{\mu\lambda}k_{1\nu}+g_2g_{\mu\lambda}p_{1\nu}+g_3g_{\nu\lambda}k_{1\mu}+g_4g_{\nu\lambda}p_{2\mu}+g_5g_{\mu\nu}p_{1\lambda}+g_6g_{\mu\nu}p_{2\lambda}$$
$$+g_7\epsilon_{\mu\nu p_1p_2}p_{1\lambda}+g_8\epsilon_{\mu\nu p_1p_2}p_{2\lambda}+g_9\epsilon_{k_1\mu\nu\lambda}+g_{10}\epsilon_{\mu\nu\lambda p_1}+g_{11}\epsilon_{\mu\nu\lambda p_2}+g_{12}\epsilon_{k_1\lambda p_1p_2}g_{\mu\nu}+g_{13}\epsilon_{k_1\nu p_1p_2}g_{\mu\lambda}$$
$$+g_{14}\epsilon_{k_1\mu p_1p_2}g_{\nu\lambda}+g_{15}\epsilon_{\nu\lambda p_1p_2}k_{1\mu}+g_{16}\epsilon_{k_1\mu\lambda p_1}k_{1\nu}+g_{17}\epsilon_{k_1\mu\lambda p_2}k_{1\nu}+g_{18}\epsilon_{\mu\lambda p_1p_2}k_{1\nu}+g_{19}\epsilon_{k_1\mu\lambda p_1}p_{1\nu}+g_{20}\epsilon_{k_1\mu\lambda p_2}p_{1\nu}$$
$$+g_{21}\epsilon_{\mu\lambda p_1p_2}p_{1\nu}+g_{22}\epsilon_{k_1\mu\nu p_2}p_{1\lambda}+g_{23}\epsilon_{k_1\mu\nu p_1}p_{2\lambda}+g_{24}\epsilon_{k_1\mu\nu p_2}p_{2\lambda}+g_{25}\epsilon_{k_1\nu\lambda p_1}p_{2\mu}+g_{26}p_{1\nu}p_{1\lambda}p_{2\mu}+g_{27}p_{1\nu}p_{2\mu}p_{2\lambda}$$
$$+g_{28}k_{1\mu}k_{1\nu}p_{1\lambda}+g_{29}k_{1\mu}p_{1\nu}p_{1\lambda}+g_{30}k_{1\nu}\cdot p_{1\lambda}p_{2\mu}+g_{31}k_{1\mu}k_{1\nu}p_{2\lambda}+g_{32}k_{1\mu}p_{1\nu}p_{2\lambda}+g_{33}k_{1\nu}p_{2\mu}p_{2\lambda}\}$$
$$+(p_1\leftrightarrow p_2,\mu\leftrightarrow\nu,t\leftrightarrow u).$$

Now we give form factors for box diagrams. Terms of order $O(m_b^2/m_t^2)$ or higher are omitted to avoid over lengthy expressions. However, we included all terms in our numerical calculation:

$$g_1=\frac{T_t}{2}\Big\{C_0^{b2}-2C_{11}^{b5}+\Big(m_t^2-m_W^2+\frac{\hat{s}}{2}+\hat{t}+\hat{u}\Big)D_0^{b1}-\frac{\hat{s}}{2}D_0^{b5}+\Big(m_t^2-m_W^2+\frac{\hat{s}}{2}+2\hat{t}+2\hat{u}\Big)D_{11}^{b1}+\Big(-m_t^2-m_W^2+\frac{\hat{s}}{2}+\hat{t}+\hat{u}\Big)D_{11}^{b2}$$
$$+(-m_W^2+\hat{s}+\hat{u})D_{12}^{b1}+\hat{s}D_{12}^{b2}+\Big(2m_t^2-m_W^2+\frac{\hat{s}}{2}+\hat{t}+2\hat{u}\Big)D_{12}^{b5}+(-m_W^2+\hat{s}+\hat{t})D_{13}^{b1}+(\hat{t}+\hat{u})(D_{21}^{b1}+D_{21}^{b2})+(m_W^2+\hat{t}$$
$$+2\hat{u})D_{22}^{b5}+\hat{u}D_{24}^{b1}+(\hat{s}+\hat{u})D_{24}^{b2}+(\hat{s}+2\hat{u})D_{24}^{b5}+\hat{t}D_{25}^{b1}-m_W^2(D_{24}^{b1}+D_{25}^{b1})+\hat{s}(D_{24}^{b1}+D_{25}^{b1})+(\hat{s}+\hat{t})(D_{25}^{b2}+2D_{26}^{b5})$$
$$-m_W^2(D_{24}^{b2}+D_{25}^{b2})-2m_W^2(D_{24}^{b5}+D_{26}^{b5})+2D_{27}^{b1}-6D_{27}^{b2}-4D_{27}^{b5}+4(D_{311}^{b1}-D_{311}^{b2}+D_{312}^{b5})\Big\}+F_1[D_{27}^{s2}+D_{311}^{s2}]-F_2[D_{27}^{s1}$$
$$+D_{311}^{s1}+D_{312}^{s5}],$$

$$g_2=\frac{T_t}{2}\Big\{-C_0^{b1}+C_{12}^{b1}+C_{12}^{b2}+2C_{12}^{b5}+(m_W^2/2+\hat{u}/2)D_0^{b1}+\Big(m_W^2/2-\frac{\hat{u}}{2}\Big)\cdot D_0^{b5}+\Big[(3m_W^2)/2+\frac{\hat{u}}{2}\Big]D_{11}^{b1}+\Big(-m_W^2/2+\frac{\hat{u}}{2}\Big)D_{11}^{b2}$$
$$+(-m_W^2+\hat{u})D_{12}^{b1}+\Big(m_W^2/2-\frac{\hat{u}}{2}\Big)D_{12}^{b5}+m_t^2(D_0^{b1}-D_{13}^{b1})+(m_t^2-\hat{u})D_{13}^{b2}+(-2m_t^2+m_W^2-\hat{s}-\hat{t}-2\hat{u})D_{13}^{b5}+(m_W^2-\hat{s}-\hat{t})$$
$$\times(D_{23}^{b1}+D_{23}^{b2}+2D_{23}^{b5})-\hat{t}D_{25}^{b1}-(\hat{t}+\hat{u})D_{25}^{b2}+(2m_W^2-\hat{s}-2\hat{u})D_{25}^{b5}+(m_W^2-\hat{s})D_{26}^{b1}-\hat{u}(D_{13}^{b1}+D_{25}^{b1}+D_{26}^{b1})+(m_W^2-\hat{s}$$
$$-\hat{u})D_{26}^{b2}+(-m_W^2-\hat{t}-2\hat{u})D_{26}^{b5}+2(D_{27}^{b1}+D_{27}^{b2}+D_{27}^{b5})+4(-D_{313}^{b1}+D_{313}^{b2}-D_{313}^{b5})\Big\}-F_1[D_{313}^{s2}]+F_2[D_{313}^{s1}+D_{313}^{s5}],$$

$$g_3=\frac{T_t}{2}\Big\{-C_0^{b2}+\Big(m_t^2+m_W^2-\frac{\hat{s}}{2}\Big)D_0^{b1}+\Big(-m_W^2+\frac{\hat{s}}{2}+\hat{u}\Big)D_0^{b5}+\Big(3m_W^2-\frac{\hat{s}}{2}\Big)D_{11}^{b1}-\Big(m_W^2+\frac{\hat{s}}{2}\Big)D_{11}^{b2}+m_t^2(D_{11}^{b1}+D_{11}^{b2})+(-m_W^2$$
$$+\hat{u})(D_{12}^{b1}+D_{22}^{b5}+D_{24}^{b1}-D_{24}^{b2})+\Big(-2m_W^2+\frac{\hat{s}}{2}+2\hat{u}\Big)D_{12}^{b5}+(-m_W^2+\hat{t})(D_{13}^{b1}+D_{25}^{b1})+\hat{s}(D_{13}^{b2}+D_{13}^{b5})+2m_W^2(D_{21}^{b1}-D_{21}^{b2})$$
$$-D_{25}^{b2})+\hat{s}D_{26}^{b5}+2D_{27}^{b1}-2D_{27}^{b2}+4(D_{27}^{b5}+D_{311}^{b1}-D_{311}^{b2}+D_{312}^{b5})\Big\}+F_1[D_{27}^{s2}+D_{311}^{s2}]-F_2[D_{27}^{s1}+D_{27}^{s5}+D_{311}^{s1}+D_{312}^{s5}],$$

$$g_4=\frac{T_t}{2}\Big\{2C_0^{b1}-C_0^{b5}+C_{11}^{b1}-C_{11}^{b2}+\Big(-2m_t^2-m_W^2/2-\frac{\hat{t}}{2}-\hat{u}\Big)D_0^{b1}+\Big(m_t^2+m_W^2/2+\frac{\hat{t}}{2}\Big)D_0^{b5}-\Big(5m_W^2/2+\frac{\hat{t}}{2}+\hat{u}\Big)D_{11}^{b1}$$
$$+\Big(3m_W^2/2-\frac{\hat{t}}{2}-\hat{u}\Big)D_{11}^{b2}+(-m_t^2+m_W^2-2\hat{u})D_{12}^{b1}-m_t^2D_{12}^{b2}+\Big(3m_W^2/2+\frac{\hat{t}}{2}\Big)D_{12}^{b5}+(2m_W^2-\hat{s}-2\hat{t})D_{13}^{b1}-\hat{s}D_{13}^{b2}+(-m_W^2$$
$$+\hat{t})(D_{13}^{b5}-D_{26}^{b1}+D_{26}^{b2})+(m_W^2-\hat{u})(D_{22}^{b1}+D_{24}^{b5})+\hat{u}(D_{12}^{b2}+D_{22}^{b2})-m_W^2(D_{22}^{b2}+2D_{24}^{b1}-2D_{24}^{b2})-\hat{s}D_{25}^{b5}-2D_{27}^{b5}-4(D_{27}^{b1}$$
$$-D_{27}^{b2}+D_{311}^{b5}+D_{312}^{b1}-D_{312}^{b2})\Big\}-F_1[D_{27}^{s2}+D_{312}^{s2}]+F_2[D_{27}^{s1}+D_{27}^{s5}+D_{311}^{s5}+D_{312}^{s1}],$$

$$g_5=\frac{T_t}{2}\Big\{C_0^{b1}+C_{12}^{b1}-C_{12}^{b2}+\Big(-m_W^2/2-\frac{\hat{u}}{2}\Big)D_0^{b1}+\Big[(-3m_W^2)/2-\frac{\hat{u}}{2}\Big]D_{11}^{b1}+\Big(m_W^2/2-\frac{\hat{u}}{2}\Big)D_{11}^{b2}+(m_W^2-\hat{u})D_{12}^{b1}-m_W^2/2(D_0^{b5}$$
$$+D_{12}^{b5})+\frac{\hat{u}}{2}(D_0^{b5}+D_{12}^{b5})+(m_W^2-\hat{s}-\hat{t}-\hat{u})D_{13}^{b1}-m_t^2(D_0^{b1}+D_{13}^{b1})-m_t^2D_{13}^{b2}+(m_W^2-\hat{s}-\hat{t})(D_{23}^{b1}-D_{23}^{b2})+(-m_W^2-\hat{u})D_{25}^{b1}$$
$$+(m_W^2-\hat{u})D_{26}^{b1}+m_W^2(D_{25}^{b2}-D_{26}^{b2})+\hat{u}(D_{13}^{b2}+D_{25}^{b2}+D_{26}^{b2})-2(D_{27}^{b1}+D_{27}^{b2}+D_{27}^{b5})+4(-D_{313}^{b1}+D_{313}^{b2}-D_{313}^{b5})\Big\}-F_1[D_{313}^{s2}]$$
$$+F_2[D_{313}^{s1}+D_{313}^{s5}],$$

$$g_6=\frac{T_t}{2}\Big[C_0^{b5}+C_{11}^{b1}-C_{11}^{b2}+\Big(-m_W^2/2+\frac{\hat{t}}{2}\Big)D_0^{b1}+\Big(-m_t^2+m_W^2/2-\hat{s}-\frac{\hat{t}}{2}-\hat{u}\Big)D_0^{b5}+\Big(-m_W^2/2+\frac{\hat{t}}{2}\Big)(D_{11}^{b1}+D_{11}^{b2})+(m_W^2-\hat{s}$$
$$-\hat{u})(D_{11}^{b5}-D_{12}^{b2})-\Big(m_W^2/2+\frac{\hat{t}}{2}+\hat{u}\Big)D_{12}^{b5}-m_t^2D_{12}^{b1}+(m_W^2-\hat{s}-\hat{t})(D_{13}^{b5}+D_{26}^{b1})+m_W^2(D_{22}^{b1}-D_{24}^{b1}-D_{22}^{b2}+D_{24}^{b2}-D_{26}^{b2})$$
$$-6D_{27}^{b5}-\hat{u}(D_{12}^{b1}+D_{22}^{b1}+D_{24}^{b1}-D_{22}^{b2}-D_{24}^{b2})+(\hat{s}+\hat{t})D_{26}^{b2}-4(D_{27}^{b2}+D_{311}^{b5}+D_{312}^{b1}-D_{312}^{b2})\Big]-F_1[D_{312}^{s2}]+F_2[D_{27}^{s5}+D_{311}^{s5}$$
$$+D_{312}^{s1}],$$

$$g_7=iT_t(D_{13}^{b1}+D_{13}^{b5}+D_{23}^{b1}+D_{23}^{b2}+D_{23}^{b5}),$$

$$g_8=iT_t(D_0^{b5}+D_{11}^{b5}-D_{12}^{b2}+D_{13}^{b1}+D_{13}^{b2}+D_{13}^{b5}+D_{25}^{b5}+D_{26}^{b1}+D_{26}^{b2}),$$

$$g_9=i\frac{T_t}{2}\Big[-C_0^{b2}+\Big(-m_t^2-m_W^2+\frac{\hat{s}}{2}\Big)D_0^{b1}+\Big(-m_W^2+\frac{\hat{s}}{2}+\hat{u}\Big)D_0^{b5}+\Big(-m_t^2-3m_W^2+\frac{\hat{s}}{2}\Big)D_{11}^{b1}+\Big(m_t^2-m_W^2+\frac{\hat{s}}{2}\Big)D_{11}^{b2}+(m_W^2-\hat{u})$$
$$\times(D_{12}^{b1}-D_{22}^{b5}+D_{24}^{b1}+D_{24}^{b2})+\Big(-2m_W^2+\frac{\hat{s}}{2}+2\hat{u}\Big)D_{12}^{b5}+(m_W^2-\hat{t})(D_{25}^{b1}+D_{25}^{b2}+D_{13}^{b1})+\hat{s}D_{13}^{b5}-2m_W^2(D_{21}^{b1}+D_{21}^{b2})+\hat{s}D_{26}^{b5}$$
$$+2(D_{27}^{b1}+D_{27}^{b2})\Big],$$

$$g_{10}=i\frac{T_t}{2}\Big\{C_0^{b1}+C_{12}^{b1}+C_{12}^{b2}+\Big(-m_t^2-m_W^2/2-\frac{\hat{u}}{2}\Big)D_0^{b1}+\Big(-m_W^2/2+\frac{\hat{u}}{2}\Big)D_0^{b5}+\Big(-3m_W^2/2-\frac{\hat{u}}{2}\Big)D_{11}^{b1}+\Big(m_W^2/2-\frac{\hat{u}}{2}\Big)D_{11}^{b2}+(m_W^2$$
$$-\hat{u})D_{12}^{b1}+\Big(-m_W^2/2+\frac{\hat{u}}{2}\Big)D_{12}^{b5}-(m_t^2+\hat{t})D_{13}^{b1}+(m_t^2-m_W^2)D_{13}^{b2}+(-m_W^2+\hat{s}+\hat{u})D_{13}^{b5}+(m_W^2-\hat{t})D_{23}^{b1}+(m_W^2-\hat{t})D_{23}^{b2}$$
$$+\hat{s}D_{23}^{b5}-2m_W^2D_{25}^{b1}-2m_W^2D_{25}^{b2}+(m_W^2-\hat{u})D_{26}^{b1}+(m_W^2-\hat{u})D_{26}^{b2}+(-m_W^2+\hat{u})D_{26}^{b5}-2(D_{27}^{b1}+D_{27}^{b2}+D_{27}^{b5})\Big\},$$

$$g_{11}=i\frac{T_t}{2}\Big\{2C_0^{b1}+2C_0^{b2}+C_0^{b5}+C_{11}^{b1}+C_{11}^{b2}+\Big(-2m_t^2-m_W^2/2-\frac{\hat{t}}{2}-\hat{u}\Big)D_0^{b1}-\Big(m_t^2+m_W^2/2+\frac{\hat{t}}{2}\Big)D_0^{b5}-\Big(5m_W^2/2+\frac{\hat{t}}{2}+\hat{u}\Big)D_{11}^{b1}$$
$$-\Big(m_W^2/2+\frac{\hat{t}}{2}+\hat{u}\Big)D_{11}^{b2}+(m_W^2-2\hat{u})D_{12}^{b1}-\hat{u}D_{12}^{b2}-\Big(3m_W^2/2+\frac{\hat{t}}{2}\Big)D_{12}^{b5}+(2m_W^2-\hat{s}-2\hat{t})D_{13}^{b1}+(m_W^2-\hat{s}-\hat{t})D_{13}^{b2}+(m_W^2$$
$$-\hat{t})(D_{13}^{b5}+D_{26}^{b2}+D_{26}^{b1})+(m_W^2-\hat{u})(D_{22}^{b1}+D_{22}^{b2}-D_{24}^{b5})-2m_W^2(D_{24}^{b1}+D_{24}^{b2})+\hat{s}D_{25}^{b5}-m_t^2D_{12}^{b1}+m_t^2D_{12}^{b2}-4(D_{27}^{b1}-D_{27}^{b2})$$
$$-6D_{27}^{b5}\Big\},$$

$$g_{12}=-g_{13}=-g_{15}=-g_{25}=i\frac{T_t}{2}(D_0^{b1}+D_0^{b5}+D_{11}^{b1}-D_{11}^{b2}+D_{12}^{b5}),$$

$$g_{14}=g_{23}=-i\frac{T_t}{2}(D_0^{b1}-D_0^{b5}+D_{11}^{b1}+D_{11}^{b2}-D_{12}^{b5}),$$

$$g_{16}=-iT_t(D_0^{b1}+2D_{11}^{b1}+D_{11}^{b2}+D_{12}^{b5}+D_{21}^{b1}+D_{21}^{b2}+D_{22}^{b5}),$$

$$g_{17}=-iT_t(D_0^{b1}+D_0^{b5}+2D_{11}^{b1}+D_{11}^{b2}+2D_{12}^{b5}+D_{21}^{b1}+D_{21}^{b2}+D_{22}^{b5}),$$

$$g_{18}=i\frac{T_t}{2}[-D_0^{b1}+D_0^{b5}-D_{11}^{b1}-D_{11}^{b2}-2D_{12}^{b1}-2D_{12}^{b2}-D_{12}^{b5}+2(D_{13}^{b1}+D_{13}^{b2}+D_{13}^{b5}-D_{24}^{b1}-D_{24}^{b2}-D_{24}^{b5}+D_{25}^{b1}+D_{25}^{b2}+D_{26}^{b5})],$$

$$g_{19}=iT_t(D_{13}^{b1}+D_{13}^{b5}+D_{25}^{b1}+D_{25}^{b2}+D_{26}^{b5}),$$

$$g_{20}=-g22=i\frac{T_t}{2}[D_0^{b1}+D_0^{b5}+D_{11}^{b1}+D_{11}^{b2}+D_{12}^{b5}+2(D_{13}^{b1}+D_{13}^{b5}+D_{25}^{b1}+D_{25}^{b2}+D_{26}^{b5})],$$

$$g_{21}=-iT_t(D_{23}^{b1}+D_{23}^{b2}+D_{23}^{b5}-D_{25}^{b5}-D_{26}^{b1}-D_{26}^{b2}),$$

$$g_{24}=-iT_t(D_0^{b1}+D_0^{b5}+D_{11}^{b1}+D_{11}^{b2}+D_{11}^{b5}+D_{12}^{b1}+D_{12}^{b5}+D_{24}^{b1}+D_{24}^{b2}+D_{24}^{b5}),$$

$$g_{26}=T_t[D_{13}^{b1}+D_{13}^{b5}+2D_{23}^{b1}-2D_{23}^{b2}+2D_{23}^{b5}+D_{25}^{b5}+D_{26}^{b1}+D_{26}^{b2}+2(D_{37}^{b5}+D_{39}^{b1}-D_{39}^{b2})]+F_1[D_{23}^{s2}+D_{39}^{s2}]-F_2[D_{23}^{s1}+D_{23}^{s5}+D_{37}^{s5}+D_{39}^{s1}],$$

$$g_{27}=T_t[D_0^{b5}+D_{11}^{b5}-D_{12}^{b2}+D_{13}^{b1}+D_{13}^{b2}+3D_{13}^{b5}+5D_{25}^{b5}+3D_{26}^{b1}-D_{26}^{b2}+2(D_{35}^{b5}+D_{38}^{b1}-D_{38}^{b2})]+F_1[D_{26}^{s2}+D_{38}^{s2}]-F_2[D_{13}^{s5}+2D_{25}^{s5}+D_{26}^{s1}+D_{35}^{s5}+D_{38}^{s1}],$$

$$g_{28}=T_t[D_0^{b1}+2D_{11}^{b1}+D_{11}^{b2}+D_{12}^{b5}+2D_{13}^{b1}-2D_{13}^{b2}+D_{21}^{b1}+D_{21}^{b2}+D_{22}^{b5}+4D_{25}^{b1}-4D_{25}^{b2}+2D_{26}^{b5}+2D_{35}^{b1}-2D_{35}^{b2}+2D_{38}^{b5}]+F_1[D_{13}^{s2}+2D_{25}^{s2}+D_{35}^{s2}]-F_2[D_{13}^{s1}+2D_{25}^{s1}+D_{26}^{s5}+D_{35}^{s1}+D_{38}^{s5}],$$

$$g_{29}=T_t[-D_{13}^{b1}-D_{13}^{b5}-2D_{23}^{b1}+2D_{23}^{b2}-2D_{23}^{b5}-D_{25}^{b1}-D_{25}^{b2}-D_{26}^{b5}-2(D_{37}^{b1}-D_{37}^{b2}+D_{39}^{b5})]-F_1[D_{23}^{s2}+D_{37}^{s2}]+F_2[D_{23}^{s1}+D_{23}^{s5}+D_{37}^{s1}+D_{39}^{s5}],$$

$$g_{30}=\frac{T_t}{2}[-D_0^{b1}+D_0^{b5}-D_{11}^{b1}-D_{11}^{b2}-2(D_{12}^{b1}+D_{12}^{b2})-D_{12}^{b5}-2(D_{24}^{b1}+D_{24}^{b2}+D_{24}^{b5})-4(D_{13}^{b1}-D_{13}^{b2}+D_{25}^{b1}-D_{25}^{b2}+D_{26}^{b1}-D_{26}^{b2}+D_{26}^{b5}+D_{310}^{b1}-D_{310}^{b2}+D_{310}^{b5})]-F_1[D_{13}^{s2}+D_{25}^{s2}+D_{26}^{s2}+D_{310}^{s2}]+F_2[D_{13}^{s1}+D_{25}^{s1}+D_{26}^{s1}+D_{26}^{s5}+D_{310}^{s1}+D_{310}^{s5}],$$

$$g_{31}=T_t[D_0^{b1}+D_0^{b5}+2D_{11}^{b1}+D_{11}^{b2}+2D_{12}^{b1}-2D_{12}^{b2}+4D_{12}^{b5}+D_{21}^{b1}+D_{21}^{b2}+3D_{22}^{b5}+4D_{24}^{b1}-4D_{24}^{b2}+2D_{24}^{b5}+2D_{34}^{b1}-2D_{34}^{b2}+2D_{36}^{b5}]+F_1[D_{12}^{s2}+2D_{24}^{s2}+D_{34}^{s2}]-F_2[D_{12}^{s1}+D_{12}^{s5}+D_{22}^{s5}+2D_{24}^{s1}+D_{24}^{s5}+D_{34}^{s1}+D_{36}^{s5}],$$

$$g_{32}=\frac{T_t}{2}[D_0^{b1}-D_0^{b5}+D_{11}^{b1}+D_{11}^{b2}-D_{12}^{b5}-2D_{13}^{b1}-2D_{13}^{b2}-6D_{13}^{b5}-2D_{25}^{b1}-2D_{25}^{b2}-4D_{25}^{b5}-4D_{26}^{b1}+4D_{26}^{b2}-6D_{26}^{b5}-4(D_{310}^{b1}-D_{310}^{b2}+D_{310}^{b5})]-F_1[D_{26}^{s2}+D_{310}^{s2}]+F_2[D_{13}^{s5}+D_{25}^{s5}+D_{26}^{s1}+D_{26}^{s5}+D_{310}^{s1}+D_{310}^{s5}],$$

$$g_{33}=T_t[-D_0^{b1}-D_0^{b5}-D_{11}^{b1}-D_{11}^{b2}-D_{11}^{b5}-3D_{12}^{b1}+2D_{12}^{b2}-3D_{12}^{b5}-2D_{22}^{b1}+2D_{22}^{b2}-3D_{24}^{b1}+D_{24}^{b2}-5D_{24}^{b5}-2(D_{34}^{b5}+D_{36}^{b1}-D_{36}^{b2})]-F_1[D_{12}^{s2}+D_{22}^{s2}+D_{24}^{s2}+D_{36}^{s2}]+F_2[D_{12}^{s1}+D_{12}^{s5}+D_{22}^{s1}+D_{24}^{s1}+2D_{24}^{s5}+D_{34}^{s5}+D_{36}^{s1}].$$

In the above expressions we adopted the definitions of one-loop integral functions in Ref. [25] and defined $d=4-\epsilon$. The numerical calculation of the vector and tensor loop integral functions can be traced back to four scalar loop integrals A_0, B_0, C_0, D_0 as shown in the Ref. [26].

[1] S. L. Glashow, Nucl. Phys. **22**, 579 (1961); S. Weinberg, Phys. Rev. Lett. **1**, 1264 (1967); A. Salam, in *Elementary Particle Theory: Relativistic Groups and Analyticity (Nobel Symposium No. 8)*, edited by N. Svartholm (Almqist and Wiksell, Stockholm, 1968), p. 367; H. D. Politzer, Phys. Rep. **14**, 129 (1974).

[2] P. W. Higgs, Phys. Lett. **12**, 132 (1964); Phys. Rev. Lett. **13**, 508 (1964); Phys. Rev. **145**, 1156 (1966); F. Englert and R. Brout, Phys. Rev. Lett. **13**, 321 (1964); G. S. Guralnik, C. R. Hagen, and T. W. B. Kibble, *ibid.* **13**, 585 (1964); T. W. B. Kibble, Phys. Rev. **155**, 1554 (1967).

[3] H. E. Haber and G. L. Kane, Phys. Rep. **117**, 75 (1985).

[4] J. Gunion, H. Haber, G. Kane, and S. Dawson, *The Higgs Hunter's Guide* (Addison-Wesley, Reading, 1990).

[5] H. E. Haber and G. L. Kane, Phys. Rep. **117**, 75 (1985).

[6] K. A. Assamagan *et al.*, ''The Higgs Working Group: Summary Report,'' hep-ph/0002258, and the references therein.

[7] J. F. Gunion, H. E. Haber, F. E. Paige, W.-K. Tung, and S. S. D. Willenbrock, Nucl. Phys. **B294**, 621 (1987).

[8] J. L. Diaz-Cruz and O. A. Sampayo, Phys. Rev. D **50**, 6820 (1994).

[9] S. Moretti and K. Odagiri, Phys. Rev. D **55**, 5627 (1997).

[10] N. G. Deshpande, X. Tata, and D. A. Dicus, Phys. Rev. D **29**, 1527 (1984); E. Eichten, I. Hinchliffe, K. Lane, and C. Quigg, Rev. Mod. Phys. **56**, 579 (1984); **58**, 1065(E) (1986).

[11] S. S. D. Willenbrock, Phys. Rev. **35**, 173 (1987); Y. Jiang, W. G. Ma, L. Han, M. Han, and Z. H. Yu, J. Phys. G **24**, 83 (1998); A. Krause, T. Plehn, M. Spira, and P. M. Zerwas, Nucl. Phys. **B519**, 85 (1998).

[12] S. Moretti and K. Odagiri, Phys. Rev. D **59**, 055008 (1999).

[13] D. A. Dicus, J. L. Hewett, C. Kao, and T. G. Rizzo, Phys. Rev. D **40**, 787 (1989).

[14] A. A. Barrientos Bendezu and B. A. Kniehl, Phys. Rev. D **59**, 015009 (1998).

[15] A. A. Barrientos Bendezu and B. A. Kniehl, Phys. Rev. D **61**, 097701 (2000).

[16] Y. S. Yang, C. S. Li, L. G. Jin, and S. H. Zhu, Phys. Rev. D **62**, 095012 (2000).

[17] M. Drees and S. P. Martin, hep-ph/9504324.

[18] J. Ellis and S. Rudaz, Phys. Lett. **128B**, 248 (1983); F. Gunion and H. E. Haber, Nucl. Phys. **B272**, 1 (1986).

[19] Particle Data Group, L. Montanet, *et al.*, Phys. Rev. D **50**, 1173 (1994); D. Schaile, CERN-PPE/94-162, 1994.

[20] W. Beenakker, A. Denner, W. Hollik, R. Mertig, T. Sack, and D. Wackeroth, Nucl. Phys. **B411**, 343 (1994).

[21] L. de Barbaro *et al.*, ''Parton Distributions Working Group,'' hep-ph/0006300, and the references herein.

[22] M. Spira, Nucl. Instrum. Methods Phys. Res. A **389**, 357 (1997); A. Djouadi, J. Kalinowski, and M. Spira, Comput. Phys. Commun. **108**, 56 (1998).

[23] V. Barger, M. S. Berger, and P. Ohmann, Phys. Rev. D **47**, 1093 (1993); **47**, 2038 (1993); V. Barger, M. S. Berger, P. Ohmann, and R. J. N. Phillips, Phys. Lett. B **314**, 351 (1993); V. Barger, M. S. Berger, and P. Ohmann, Phys. Rev. D **49**, 4908 (1994).

[24] A. A. Barrientos Bendezu and B. A. Kniehl, ''Squark loop correction to $W^{\pm}H^{\mp}$ associated hadron production,'' hep-ph/0007336.

[25] Bernd A. Kniehl, Phys. Rep. **240**, 211 (1994).

[26] G. Passarino and M. Veltman, Nucl. Phys. **B160**, 151 (1979).